Model Predictive Control based Coordinated Control for Free-Flying Space Manipulator Systems

Peter Kötting *

* *Institute of System Dynamics and Control, German Aerospace Center (DLR), 82234 Weßling, Germany (e-mail: Peter.Koetting@dlr.de)*

Abstract: Space Manipulator Systems (SMS) used in On-Orbit Servicing (OOS) missions are over-actuated, and safety critical systems that perform complex tasks in space. We propose a coordinated control for a free-flying SMS, which is based on a cascaded output tracking nonlinear model predictive control, to simultaneously control the spacecraft-base and manipulator of the SMS. The output tracks a given end-effector pose trajectory, and by using an artificial reference the controller stays feasible even for an unreachable trajectory. Moreover, the systems over-actuation is optimally resolved, such that the base of the SMS can be utilized to generate an unrestricted workspace for robotic operations. Throughout the entire mission, critical constraints related to system and safety, including collision avoidance, field of view of sensor devices, joint limitations, and actuator saturations, are integrated as hard constraints. Simulations of the most challenging mission phases, such as the approach and detumbling of a target spacecraft, as well as an escape maneuver verify the performance, reliability, and flexibility of our coordinated control concept.

Keywords: Model Predictive Control, Coordinated Control, On-Orbit Servicing, Space Robotics, Redundant Robots, Motion Control

1. INTRODUCTION

Robotic system capabilities for On-Orbit Servicing (OOS) are a key component for further space exploration and exploitation. This key technology can enable additional mission tasks such as inspecting, refueling, upgrading, repairing satellites, removing debris, maintenance, and constructing large orbital structures since these tasks are often costly, risky, or inaccessible for astronaut extravehicular activities. Typically, a Space Manipulator System (SMS) consists of a spacecraft base equipped with a robotic manipulator, as shown in Fig. 1. Accordingly, SMS are over-actuated systems which in addition to joint motors generates motion in space by spacecraft actuators, such as thrusters and momentum wheels.

First SMS control strategies were focused on commanding the manipulator while deactivating the spacecraft's actuators, known as a *free-floating* approach (Vafa and Dubowsky (1990); Masutani et al. (1993)). This approach has the advantage of reducing fuel consumption. OOS missions often require spacecraft attitude control due to the limited field of view (FoV) of sensor devices for navigation, which is not addressed by the free-floating approach. Additionally, this approach faced challenges such as dynamic singularities and a restricted workspace since the spacecraft's pose is not controlled. To address these issues, coordinated control strategies were developed for a *free-flying* approach, where all SMS actuators, including spacecraft actuators and joint drivers, are controlled simultaneously. Various techniques were proposed within these coordinated control strategies. For example, in (Xu and Kanade (1993)) an adaptive scheme is introduced, while in (Aghili (2009)) a feedback linearization is employed to control the spacecraft's attitude and the end effector's position. Indeed, these methods are not stabilizing the base position, which could result to a drifting motion during contact. Additionally, the workspace is restricted to the manipulator capabilities. By a transposed Jacobian approach (Papadopoulos and Dubowsky (1991)) all actuators are controlled. An alternative coordinated control, as proposed by (Giordano et al. (2019)), suggests regulating the translation of the SMS center of mass (CoM), which allows free translation of the geometric center and decoupling of the control tasks, leading to reduced thruster usage. Another challenge in OOS missions is the multi-rate stability issue, which is not addressed by prior approaches. Typically, the control of the servicer base operates at a slow sampling rate, e.g., 10 Hz, while the manipulator controller operates at a higher rate, e.g., 1000 Hz. A

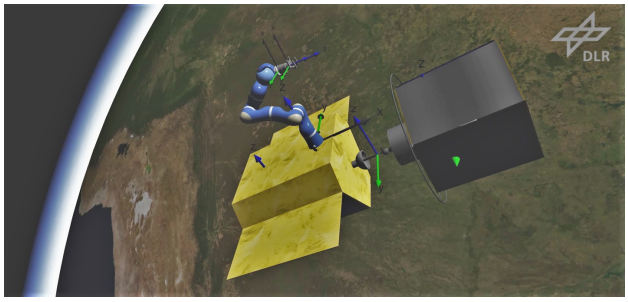

Fig. 1. On-Orbit Servicing Scenario with a Space Manipulator System (left) and a Target Spacecraft (right).

multi-rate tracking control technique has been developed by (De Stefano et al. (2019)) by using the time-domain passivity approach.

However, none of these control approaches considers the optimal usage of the system over-actuation and satisfaction of constraints. Therefore, the current approaches require a trajectory planner capable of computing trajectories for every system state, ensuring adherence to all constraints and optimally resolving the over-actuation. This leads to open issues: (i) State constraints can only be satisfied for the reference values and the inputs computed by the controller cannot be explicitly constrained, (ii) A trajectory planner considering the robotic system dynamics with system and safety constraints over the whole mission trajectories results in a nonlinear optimization problem with very high computational demand (Lampariello and Hirzinger (2013)), which needs to be partially solved offline comprising a limited set of spinning/tumbling target states and target geometry.

Contribution This paper formulates the control problem from another perspective by only assuming a high level end-effector trajectory. Accordingly, complexity for optimization is shifted from the trajectory planning to the control system. By using Model Predictive Control (MPC), we optimize for a short prediction horizon N allowing for real-time solutions without precomputing the entire mission phases. We propose an output tracking nonlinear MPC to follow the end-effector reference pose while an artificial reference serves as a joint space reference for optimal usage of the over-actuation. System and safety constraints, such as Collision Avoidance (CA), FoV of sensor devices, and joint angle limits are explicitly integrated by state constraints. Actuator limits, such as thruster saturation, momentum wheel torque limits and joint limits are also explicitly integrated as input constraints. The resulting complexity is handled by proposing a novel cascaded schema in which the MPC based coordinated control serves as a top-layer control with a subordinate joint space control, as shown in Fig. 2. Accordingly, we separate the fast joint space dynamics from the whole system description to solve the multi-rate stability issue by designing a fast joint space control and a slow discrete MPC based coordinated control. To the best knowledge of the author, the development of such a coordination control concept for an SMS has not yet been investigated.

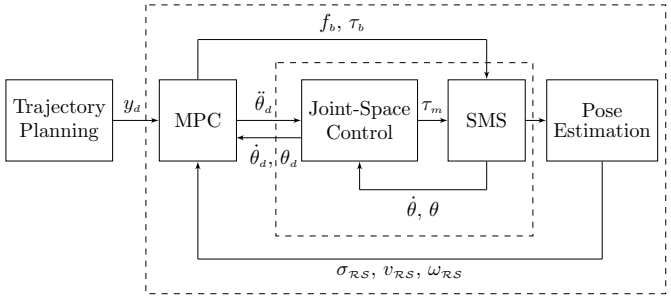

Fig. 2. Coordinated control structure, with an inner joint space control lop (1000 Hz) and a MPC based coordinated control outer loop (10 Hz). The SMS represents the multi-body system with actuators and sensors.

2. SYSTEM DESCRIPTION

2.1 Notations and Definitions

In the following used frames are defined: A servicer-base frame $\{\mathcal{S}\}$; an end-effector frame $\{\mathcal{E}\}$; a target object frame $\{\mathcal{T}\}$; a grasping handle frame $\{\mathcal{G}\}$; and finally, an orbital reference frame $\{\mathcal{R}\}$, placed at the target origin. The position of the origin of a general frame $\{\mathcal{Y}\}$ relative to a general frame $\{\mathcal{X}\}$ is denoted by the position vector $p_{\mathcal{XY}}$ and the orientation of frame $\{\mathcal{Y}\}$ relative to frame $\{\mathcal{X}\}$ is denoted by the rotation matrix $R_{\mathcal{XY}} \in SO(3)$. We define with $v_{\mathcal{XY}} \in \mathbb{R}^3$ and $\omega_{\mathcal{XY}} \in \mathbb{R}^3$ the translational and angular velocities of a general frame $\{\mathcal{Y}\}$ relative to a general frame $\{\mathcal{X}\}$ expressed in the frame $\{\mathcal{X}\}$, respectively. Let us further specify an identity matrix with dimension n by I_n, a zero matrix by $\mathbf{0}$, the skew-symmetric operator by $S(\cdot) : \mathbb{R}^3 \to SO(3)$, defined by the condition $S(x)y = x \times y$ for any x, $y \in \mathbb{R}^3$. The quadratic norm with respect to a positive definite matrix Q is denoted by $||x||_Q^2 = x^T Q x$.

We parameterize orientations by unit quaternions, which are defined as $q = [\eta, \epsilon^T]^T \in \mathbb{S}^3 = \{x \in \mathbb{R}^4 : x^T x = 1\}$. Consequently, we indicate by the unit quaternion $q_{\mathcal{XY}}$ the orientation of frame $\{\mathcal{Y}\}$ relative to frame $\{\mathcal{X}\}$ and the pose of frame $\{\mathcal{Y}\}$ relative to frame $\{\mathcal{X}\}$ by $\sigma_{\mathcal{XY}} = [p_{\mathcal{XY}}^T \quad q_{\mathcal{XY}}^T]^T$. We further use the quaternion propagation

$$\dot{q} = \frac{1}{2}\Xi(q)\omega, \qquad \Xi(q) = \begin{pmatrix} -\epsilon^T \\ \eta I_3 - S(\epsilon) \end{pmatrix}, \tag{1}$$

and the quaternion error

$$e_q = \eta\epsilon_d - \eta_d\epsilon - S(\epsilon_d)\epsilon. \tag{2}$$

An additional subscript d indicates desired values.

2.2 System Dynamics

We begin by considering the system dynamics of the rigid multibody model of a SMS with a n_m DoF manipulator. Accordingly, the equations of motions for a free-flying SMS can be defined by (Xu and Kanade (1993))

$$\begin{bmatrix} H_t & H_{tr} & H_{tm} \\ H_{tr}^T & H_r & H_{rm} \\ H_{tm}^T & H_{rm}^T & H_m \end{bmatrix} \begin{pmatrix} \dot{v}_{\mathcal{RS}} \\ \dot{\omega}_{\mathcal{RS}} \\ \ddot{\theta} \end{pmatrix} + \begin{pmatrix} c_b \\ c_\omega \\ c_m \end{pmatrix} = \begin{pmatrix} f_b \\ \tau_b \\ \tau_m \end{pmatrix}, \tag{3}$$

where $H \in \mathbb{R}^{(6+n_m)\times(6+n_m)}$ specifies the inertia tensor and c_b, $c_\omega \in \mathbb{R}^3$, and $c_m \in \mathbb{R}^{n_m}$ define the translational, rotational, and robotic arm non-linear Coriolis and centrifugal forces, respectively. The input vector includes the base force $f_b \in \mathbb{R}^3$, the base torque $\tau_b \in \mathbb{R}^3$, and the manipulator torques $\tau_m \in \mathbb{R}^{n_m}$. The motion of the manipulator is described by the joint angles $\theta \in \mathbb{R}^{n_m}$, velocities $\dot{\theta} \in \mathbb{R}^{n_m}$, and accelerations $\ddot{\theta} \in \mathbb{R}^{n_m}$.

One core idea of our approach is dividing the SMS dynamics (3) into slow top-layer dynamics and fast sub-layer dynamics. The top-layer dynamics considers the robot joint dynamics in its quasi-steady state, i.e., $\ddot{\theta} = \ddot{\theta}_d$, $\dot{\theta} = \dot{\theta}_d$, $\theta = \theta_d$. Based on this assumption, the system dynamics (3) of the top-layer results in

$$\underbrace{\begin{bmatrix} H_t & H_{tr} & H_{tm} \\ H_{tr}^T & H_r & H_{rm} \\ \mathbf{0} & \mathbf{0} & I_{n_m} \end{bmatrix}}_{H} \begin{pmatrix} \dot{v}_{\mathcal{RS}} \\ \dot{\omega}_{\mathcal{RS}} \\ \ddot{\theta} \end{pmatrix} + \underbrace{\begin{pmatrix} c_b \\ c_\omega \\ 0_{1\times 6} \end{pmatrix}}_{c} = \underbrace{\begin{pmatrix} f_b \\ \tau_b \\ \ddot{\theta}_d \end{pmatrix}}_{u}, \tag{4}$$

where the new input vector $u \in \mathbb{R}^m$ includes the base force f_b, the base torque τ_b, and the desired manipulator joint accelerations $\ddot{\theta}_d \in \mathbb{R}^{n_m}$. The fast dynamics is expressed by the last line of the SMS dynamics (3), i.e.,

$$H_m\ddot{\theta} + c_m + H_{tm}^T\dot{v}_{\mathcal{RS}} + H_{rm}^T\dot{\omega}_{\mathcal{RS}} = \tau_m. \tag{5}$$

Accordingly, this sub-layer dynamics (5) is controlled by the joint space control. We propose using the torque input $\tau_m = \tau_f + \tau_c$, where $\tau_f = H_{tm}^T\dot{v}_{\mathcal{RS}} + H_{rm}^T\dot{\omega}_{\mathcal{RS}}$ describes a feed forward control to compensate the coupling terms with the base. The remaining dynamics

$$H_m\ddot{\theta} + c_m = \tau_c, \tag{6}$$

describes the well investigated joint space control problem, which is already solved by a variety of state-of-the-art methods (Siciliano (2016)). Consequently, we focus in the following section on designing the coordinated control in the top-layer.

3. MPC BASED COORDINATED CONTROL

3.1 Control Problem

In this section, we begin by introducing the control problem at a generic level. Our control goal is tracking a given output reference trajectory $y_d \in \mathbb{R}^{p\times N}$. A SMS can be formulated as a nonlinear, discrete-time system

$$\begin{aligned} x_{t+1} &= f(x_t, u_t), \\ y_t &= h(x_t), \end{aligned} \tag{7}$$

with the system dynamics $f : \mathbb{R}^n \times \mathbb{R}^m \to \mathbb{R}^n$, the output function $h : \mathbb{R}^n \to \mathbb{R}^p$, the state $x \in \mathbb{R}^n$, the input $u \in \mathbb{R}^m$, the output $y \in \mathbb{R}^p$, and the discrete time $t \in \mathbb{N}$. The system is redundant, i.e., $p < m$. Furthermore, the system is subject to hard constraints on state and input

$$(x_t,\, u_t) \in \mathbb{A} \subseteq \mathbb{R}^{n\times m}, \tag{8}$$

where $\mathbb{A}$ is a closed set whose interior is not empty.

To address the constrained control of the over-actuated system, an optimization-based control approach becomes the natural choice. The distinctive advantages of MPC over alternative optimal control methods lie in its capacity to (i) effectively address the control problem with a foundation in rigorous theoretical properties, and (ii) enable a smooth reallocation between base and joint actuators, particularly in constrained scenarios, based on its explicit formulation as a predictive approach.

A nonlinear output tracking MPC schema is capable to address the formulated problem. Recent research from (Limon et al. (2018)) and (Soloperto et al. (2023)) has proposed such MPC schemes with an artificial reference. These approaches can be implemented without terminal ingredients, and are even feasible if the reference is unreachable. Tracking an unreachable final objective can improve the performance for the detumbling and escape phase as shown in Section 4. These methodologies involve calculating the artificial reference as a single steady-state to follow a piece-wise constant trajectory. We extend this approach by predicting the artificial reference for every prediction time step k, improving tracking of a generic trajectory profile.

3.2 Proposed MPC Schema

At each time t, given the current states x_t and an output reference trajectory $y_{d,t}$, the following optimization problem is solved:

$$\begin{aligned} J_N(x_t, y_{d,t}) = \min_{u_{\cdot|t}, x^s_{\cdot|t}}\ & V_N(x_{\cdot|t}, u_{\cdot|t}, y^s_{\cdot|t}, x^s_{\cdot|t}, y_{d,t}) \\ s.t.\quad & x_{0|t} = x_t, && \text{(9a)}\\ & x_{k+1|t} = f_{RK4}(x_{k|t}, u_{k|t}), && \text{(9b)}\\ & Fx_{k|t} \le f, \quad Eu_{k|t} \le e, && \text{(9c)}\\ & g_j(x_{k|t}, x^s_{k|t}, y^s_{k|t}) \le 0, && \text{(9d)}\\ & y^s_{k|t} = h(x^s_{k|t}), && \text{(9e)}\\ & x_{N|t} = x^s_{N|t}, && \text{(9f)}\\ & k = 0, ..., N-1, \quad j = 0, ..., l-1, \end{aligned}$$

with the prediction step k and the current time t. Hence, the optimization problem gets solved subject to the constraints. These are the system dynamics (9b) with the initial condition (9a), polytopic state and input constraints (9c), nonlinear state and output constraints (9d), artificial state output constraint (9e), and terminal equality constraint (9f). The solution of the optimization problem (9) contains the optimal state and input trajectory $(x^*_{\cdot|t}, u^*_{\cdot|t})$ and the optimal artificial reference state $x^{s,*}_{\cdot|t}$ and output $y^{s,*}_{\cdot|t}$. The artificial reference $x^s_{\cdot|t}$ serves as the reference for the predicted system states $x_{\cdot|t}$ and is further used as a terminal equality constraint at the prediction horizon N. The control input to be applied on the plant is the first element of the optimal input trajectory $u_t = u^*_{0|t}$.

We define the objective function by

$$\begin{aligned} &V_N(x_{\cdot|t}, u_{\cdot|t}, y^s_{\cdot|t}, x^s_{\cdot|t}, y_{d,t}) \\ &= \sum_{k=0}^{N-1} ||e_x(x_{k|t}, x^s_{k|t})||^2_Q + ||u_{k|t}||^2_R + ||e_y(y^s_{k|t}, y_{d,t})||^2_S, \end{aligned} \tag{10}$$

that consists of the terms: (i) A state stage cost penalizes the predicted state w.r.t. the artificial reference $e_x = (x_{k|t} - x^s_{k|t})$; (ii) An input stage cost penalizes the actuator usage; (iii) An output cost penalizes the tracking error stage cost between artificial reference output and the given reference trajectory $e_y = (y^s_{k|t} - y_{d,t})$. The quaternion representation can be integrated by substituting with the orientation error (2).

3.3 Prediction Model and System Output

We derive from the system dynamics (4) and the quaternion propagation (1) the state space model

$$\dot{x} = f(x,u) = \begin{pmatrix} \dot{\Omega} \\ \dot{\phi} \end{pmatrix} = \begin{pmatrix} \Gamma(\Omega)\phi \\ H(\Omega)^{-1}(u - c(\Omega, \phi)) \end{pmatrix}, \tag{11}$$

with the state

$$\begin{aligned} x &= [\Omega^T \quad \phi^T]^T \in \mathbb{R}^{n=13+2n_m}, \\ \Omega &= [p^T_{\mathcal{RS}} \quad q^T_{\mathcal{RS}} \quad \theta^T]^T \in \mathbb{R}^{7+n_m}, \\ \phi &= [v^T_{\mathcal{RS}} \quad \omega^T_{\mathcal{RS}} \quad \dot{\theta}^T]^T \in \mathbb{R}^{6+n_m}, \end{aligned}$$

including the system configuration Ω, the respective velocities ϕ, and furthermore the input

$$u = [f_b^T \quad \tau_b^T \quad \ddot{\theta}_d^T]^T \in \mathbb{R}^{m=6+n_m}.$$

Γ covers the chosen attitude representation, where we utilize unit quaternions with the propagation (1), i.e.,

$$\Gamma(\Omega) = \begin{pmatrix} I_3 & \mathbf{0} & \mathbf{0} \\ \mathbf{0} & \frac{1}{2}\Xi(q) & \mathbf{0} \\ \mathbf{0} & \mathbf{0} & I_{n_m} \end{pmatrix} \in \mathbb{R}^{(7+n_m)\times(6+n_m)}.$$

The system dynamics equality constraint (9b) is the result of applying 4th order Runge Kutta to the state space model (11).

We define the output by the end-effector pose

$$y = \sigma_{\mathcal{RE}} = \begin{pmatrix} p_{\mathcal{RE}} \\ q_{\mathcal{RE}} \end{pmatrix} = h(\Omega) \in \mathbb{R}^p, \tag{12}$$

where $h(\Omega)$ specifies the direct kinematic, which can be computed by successive homogeneous transformations along the kinematic chain of the SMS. Based on the specified output function, the artificial reference state results to $x^s_{k|t} = [\Omega^{sT}_{k|t}, 0^T_{(6+n_m)\times 1}]^T$. Thus, the predicted configuration gets penalized with respect to the artificial reference configuration, while velocities get penalized absolutely.

3.4 Constraints Formulation

Fist, we consider polytopic input and state constraints. Input constraints are taking into account the saturation of actuators, such as maximum thrust force, momentum wheel torque, and joint motor acceleration, i.e., $\bar{u} = [\bar{f}_b,\ \bar{\tau}_b,\ \ddot{\bar{\theta}}_m]$, respectively. This can be integrated by linear inequality constraints

$$Eu_{k|t} \leq e, \qquad E = \begin{bmatrix} I_m \\ -I_m \end{bmatrix}, \quad e = \begin{bmatrix} \bar{u} \\ -\bar{u} \end{bmatrix}. \tag{13}$$

Manipulator joint angle limits are also integrated by the linear inequality state constraints

$$F\theta_{k|t} \leq f, \qquad F = \begin{bmatrix} I_{n_m} \\ -I_{n_m} \end{bmatrix}, \quad f = \begin{bmatrix} \bar{\theta} \\ -\bar{\theta} \end{bmatrix}. \tag{14}$$

Second, we formulate nonlinear constraints to integrate collision avoidance and FoV of sensor devices. We approximate the obstacles with differentiable functions. Collision avoidance of the servicer base and the end-effector with an obstacle o can be realized by

$$\begin{aligned} g_1 &= ||p_{\mathcal{RS},k|t} - x^o||^2_{A^o} + b^o(p_{\mathcal{RS},k|t} - x^o) - c_{ca1} \geq 0, \\ g_2 &= ||y^s_{k|t} - x^o)||^2_{A^o} + b^o(y^s_{k|t} - x^o) - c_{ca2} \geq 0, \end{aligned} \tag{15}$$

with the parametrization $A^o \in \mathbb{R}^{3\times 3}$, $b^o \in \mathbb{R}^{1\times 3}$, and some constant c_{ca1}, $c_{ca2} \in \mathbb{R}$. FoV can be integrated by the equality constraint on the artificial reference state

$$\begin{aligned} g_3 &= a_d(p^s_{\mathcal{RS},k|t}) - a(q^s_{\mathcal{RS},k|t}) = 0, \\ a_d &= -\frac{p_{\mathcal{RS}}}{||p_{\mathcal{RS}}||^2}, \quad a = \begin{pmatrix} 2(\eta^2 + \epsilon_1^2) - 1 \\ 2(\epsilon_1\epsilon_2 + \eta\epsilon_3) \\ 2(\epsilon_1\epsilon_3 - \eta\epsilon_2) \end{pmatrix}, \end{aligned} \tag{16}$$

with the dicrection vector a and its desired counterpart a_d, aiming the servicer base in the direction towards the target

4. SIMULATION RESULTS

4.1 Scenario

System Setup: The SMS configuration applied for the simulations within this work consists of a scaled (factor 2) DLR lightweight robot mounted to a spacecraft base as depicted in Fig. 1. The servicer and target spacecraft is parameterized in Tab. 1 and the constraints in Tab. 2. For a comprehensive understanding of the manipulator, see (Hirzinger et al. (2002)). The computations are performed by using the CasADi API (Andersson et al. (2019)) and an interior point optimizer, for solving the optimization problem (9) with a 100 ms integration step and a prediction horizon $N = 30$. The reference trajectory for the end-effector is generated by the algorithm (Aghili (2009)).

Table 1. Spacecraft Parameters

Parameter	Symbol	Value	Unit
Servicer mass	m_s	1500	kg
Servicer inertia tensor	I_s	$1000\, I_3$	kg m^2
Target mass	m_t	1500	kg
Target inertia tensor	I_t	$1000\, I_3$	kg m^2

Due to limited computation performance of current space hardware, we introduce an approximation for the following simulations. OOS scenarios are characterized by slow robot motions. Accordingly, the state prediction for $k = [1, ..., N]$ stays close to the current joint space configuration, such that the dynamic term variation is relatively small. Thus, we approximate the inertia tensor and the Coriolis and centrifugal forces in the prediction model as constant over the prediction step k, i.e., $H(\Omega_{k|t}) \approx H(\Omega_{0|t})$ and $c(\Omega_{k|t}, \phi_{k|t}) \approx c(\Omega_{0|t}, \phi_{0|t})$, but varying by time t.

If the target is grasped, we assume a rigid end-effector target connection for the prediction model, such that we can map the target parameter on the robot end-effector by using the theorem of Huygens Steiner.

Table 2. Constraint Parameters

Parameter	Symbol	Value	Unit
Max thrust force	f_b	$[20\,20\,20]^T$	N
Max base torque	$\bar{\tau}_b$	$[10\,10\,10]^T$	Nm
Max joint acceleration	$\ddot{\bar{\theta}}$	$[0.1, ..., 0.1]^T$	rad/s^2
Target CA matrix	A^o	I_3	-
Target CA vector	b^o	$0_{1\times 3}$	-
Target obstacle position	x^o	$p_{\mathcal{RT}}$	-
Min CA radius for $\mathcal{S}$	c_{ca1}	3.130	m
Min CA radius for $\mathcal{E}$	c_{ca2}	1.103	m

Mission Setup: On-orbit missions with uncooperative tumbling targets are the greatest challenge. We consider the most safety-critical mission phases, defined here as benchmark examples, as follows: (i) In the approach phase the servicer approaches the target along a given end-effector trajectory, which matches the grasping point of a tumbling target in position and velocity at a certain time t_1. (ii) Followed by the gasping phase, in which the end-effector tracks synchronized the grasping point until the target is grasped at time t_2. (iii) Afterwards the motion is decelerated in the detumbling phase until the combined system is at rest at t_3. (iv) In case of an unexpected safety issues, an escape phase is triggered in which the SMS moves as fast as possible to some safe pose.

4.2 Simulation Results

Simulations based on planer trajectories are performed, to reduce the number of stats and inputs to be shown in this paper. We start by analyzing the results of an

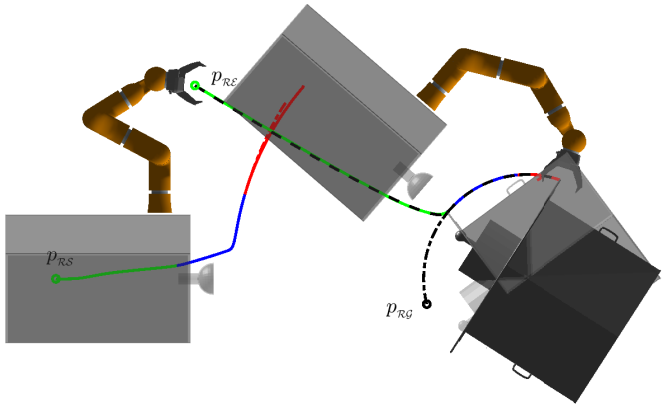

Fig. 3. **Approach and Detumbling Scenario.** y_d (black dashed) and $p_{\mathcal{RG}}$ (back dash-dotted). Closed-loop $p_{\mathcal{RE}}$ and $p_{\mathcal{RS}}$ for approach phase (green), grasping phase (blue), and detumbling phase (red), with DT1 (solid), DT2 (dot dashed).

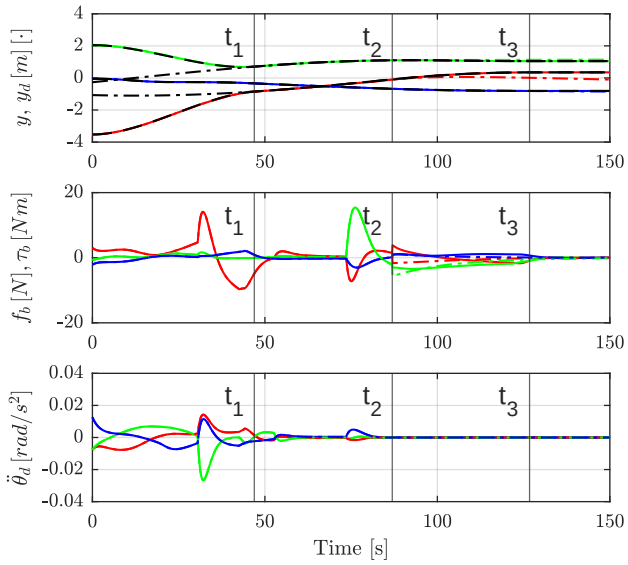

Fig. 4. **Approach and Detumbling Scenario.** DT1 (solid), DT2 (dot dashed), p_{RG} (dash-dotted). *Top:* y_d (black), $p_{\mathcal{RE}x}$ (red), $p_{\mathcal{RE}y}$ (green), $\epsilon_{\mathcal{RE}z}$ (blue). *Middle:* f_{bx} (red), f_{by} (green), τ_z (blue). *Bottom:* $\ddot{\theta}_1$ (red), $\ddot{\theta}_2$ (green), $\ddot{\theta}_3$ (blue).

approach and detumbling maneuver, which are shown in Fig. 3 and 4. The approach and subsequent synchronized movement serve as a benchmark demonstrating proper tracking and capabilities to optimally resolve the system over-actuation. According to the chosen objective function the controller moves the manipulator until it gets close to its workspace boundaries, then it smoothly reallocates to servicer base movements. Hence, we enable an unlimited workspace of the SMS. After grasping at t_2, Fig. 3 and 4 show two successfully detumbling variants, the first (DT1) is based on tracking the reference trajectory, where the second (DT2) is done by the output objective to just penalize velocities and inputs. We compare these variants

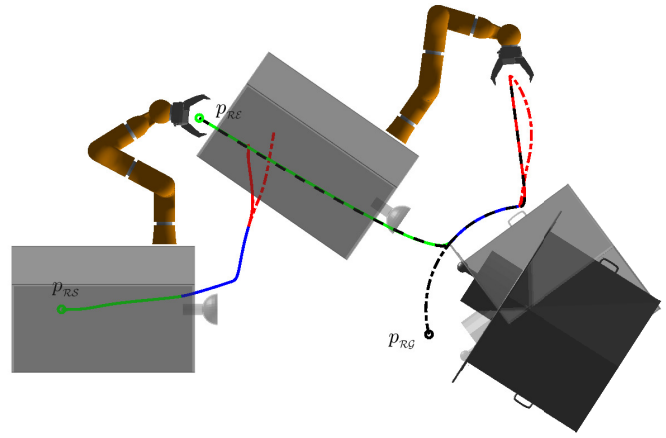

Fig. 5. **Approach and Escape Scenario.** y_d (black dashed) and $p_{\mathcal{RG}}$ (back dash-dotted). Closed-loop $p_{\mathcal{RE}}$ and $p_{\mathcal{RS}}$ for approach phase (green), grasping phase (blue), and escape phase (red), with ES1 (solid), ES2 (dot dashed).

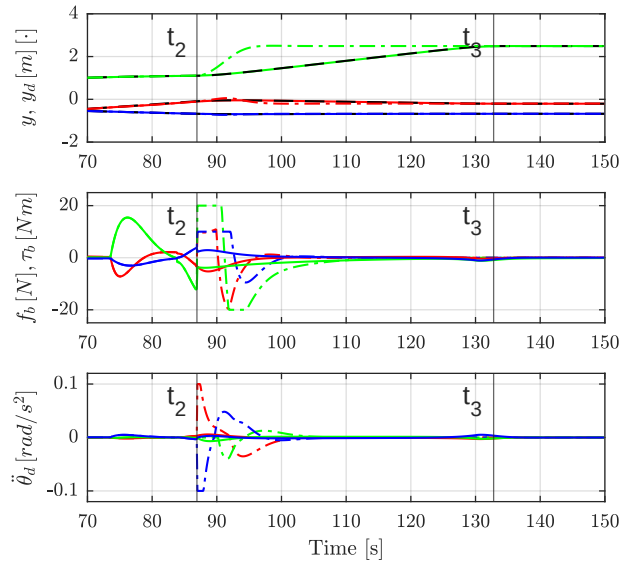

Fig. 6. **Approach and Escape Scenario.** ES1 (solid), ES2 (dot dashed). *Top:* y_d (black), $p_{\mathcal{RE}x}$ (red), $p_{\mathcal{RE}y}$ (green), $\epsilon_{\mathcal{RE}z}$ (blue). *Middle:* f_{bx} (red), f_{by} (green), τ_z (blue). *Bottom:* $\ddot{\theta}_1$ (red), $\ddot{\theta}_2$ (green), $\ddot{\theta}_3$ (blue).

based on the fuel consumption capabilities. According to a simplified fuel-consumption model, the nominal consumed fuel $c = \alpha_1 c_{tr} + \alpha_2 c_{rot} \in \mathbb{R}$, with the thruster related constants α_1, α_2 can be measured by

$$c_{tr} = \sum_{t=t_2}^{t_3} ||f_{b,0|t}||, \quad c_{rot} = \sum_{t=t_2}^{t_3} ||\tau_{b,0|t}||, \tag{17}$$

for the translation and rotation, respectively. As shown in Fig. 7 DT2 consumes 84% of the translation related fuel and only 45% of rotation related fuel. The reduction is based on the fact, that the implemented trajectory planner considers detumbling around the target CoM as

optimal, while DT2 detumbles with knowledge of the combined system CoM including SMS and target. In the special case of scenarios with small tumbling rates or targets, grasping can be performed within the manipulator workspace, i.e., without moving the base. Within such a scenario all free-flying coordinated control approaches, despite (Giordano et al. (2019)), compensate the coupling forces and moments induced by the manipulator to track a given servicer pose. Since our base position is free to move, we can avoid unnecessary thruster usage.

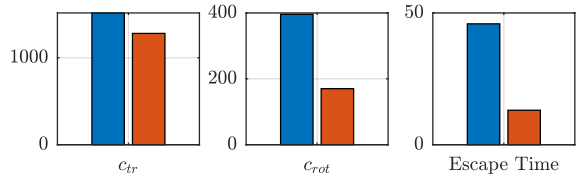

Fig. 7. Left and Middle: Detumbling phase fuel consumption with DT1 (blue) and DT2 (red). Right: Escape phase time with ES1 (blue) and ES2 (red).

As a second scenario, we consider an approach followed by an escape phase as shown in Fig. 5 and 6. The first variant (ES1) tracks the given escape trajectory $y_{d,t}$, while the second approach (ES2) tracks directly a given final constant end-effector pose y_{d,t_3}, which is possible since our MPC schema stays feasible even for a unreachable reference. The main objective within the escape phase is to move the SMS to a safe pose as fast as possible. The high-level trajectory planner cannot account for the configuration-dependent motion capabilities resulting in a conservative movement in ES1. In comparison, ES2 utilizes the full power of the actuators to their limits and moves on a path which is optimal in the robotic joint space. Consequently, as shown in Fig. 7, ES2 needs just 28% of the escape time of ES1. To summarize, the controller can be used without a trajectory planner if the reference is a constant final state, as is the case for detumbling and escape. If a trajectory needs to be tracked, as is the case when approaching a time-varying grasping point, a trajectory planning is needed.

5. CONCLUSION

This paper demonstrates the effectiveness of the proposed cascaded output tracking MPC for reliably solving the constrained coordinated control problem. Leveraging a predictive approach, we facilitate seamless coordination between the SMS base and manipulator, resulting in an unrestricted robotic workspace. In a reference scenario, the coordinated control successfully executed the approach and detumbling of a target spacecraft, as well as an escape maneuver. Our approach not only shows proper tracking results and satisfaction of system- and safety critical constraints, it is also able to reduce the fuel consumption as shown for the detumbling, and to accelerate an escape maneuver by using the full system capabilities up to the limits, but not beyond. Future work will be focused on verification and validation of this concept in hardware-in-the-loop simulations, derivation of formal properties for recursive feasibility and stability and a robust extension to include uncertainties and disturbances due to modeling simplifications and environmental effects.

REFERENCES

Aghili, F. (2009). Coordination Control of a Free-Flying Manipulator and Its Base Attitude to Capture and Detumble a Noncooperative Satellite. In *2009 IEEE/RSJ International Conference on Intelligent Robots and Systems*, 2365–2372. IEEE.

Andersson, J.A.E., Gillis, J., Horn, G., Rawlings, J.B., and Diehl, M. (2019). CasADi: a software framework for nonlinear optimization and optimal control. *Mathematical Programming Computation*, 11(1), 1–36.

De Stefano, M., Mishra, H., Balachandran, R., Lampariello, R., Ott, C., and Secchi, C. (2019). Multi-Rate Tracking Control for a Space Robot on a Controlled Satellite: A Passivity-Based Strategy. *IEEE Robotics and Automation Letters*, 4(2), 1319–1326.

Giordano, A.M., Ott, C., and Albu-Schäffer, A. (2019). Coordinated Control of Spacecraft's Attitude and End-Effector for Space Robots. *IEEE Robotics and Automation Letters*, 4(2), 2108–2115.

Hirzinger, G., Sporer, N., Albu-Schäffer, A., Hahnle, M., Krenn, R., Pascucci, A., and Schedl, M. (2002). DLR's torque-controlled light weight robot III-are we reaching the technological limits now? In *Proceedings 2002 IEEE International Conference on Robotics and Automation (Cat. No.02CH37292)*, 1710–1716. IEEE.

Lampariello, R. and Hirzinger, G. (2013). Generating Feasible Trajectories for Autonomous On-Orbit Grasping of Spinning Debris in a Useful Time. In *2013 IEEE/RSJ International Conference on Intelligent Robots and Systems*, 5652–5659. IEEE.

Limon, D., Ferramosca, A., Alvarado, I., and Alamo, T. (2018). Nonlinear MPC for Tracking Piece-Wise Constant Reference Signals. *IEEE Transactions on Automatic Control*, 63(11), 3735–3750.

Masutani, Y., Miyazaki, F., and Arimoto, S. (1993). Sensory Feedback Control for Space Manipulators. In Y. Xu and T. Kanade (eds.), *Space Robotics: Dynamics and Control*, volume 188 of *The Kluwer International Series in Engineering and Computer Science*, 205–227. Springer US, Boston, MA.

Papadopoulos, E. and Dubowsky, S. (1991). Coordinated manipulator/spacecraft motion control for space robotic systems. In *Proceedings. 1991 IEEE International Conference on Robotics and Automation*, 1696–1701. IEEE Comput. Soc. Press.

Siciliano, B. (2016). *Springer Handbook of Robotics*. Springer Handbooks Ser. Springer International Publishing AG, Cham, 2nd ed. edition.

Soloperto, R., Köhler, J., and Allgöwer, F. (2023). A Nonlinear MPC Scheme for Output Tracking Without Terminal Ingredients. *IEEE Transactions on Automatic Control*, 68(4), 2368–2375.

Vafa, Z. and Dubowsky, S. (1990). The Kinematics and Dynamics of Space Manipulators: The Virtual Manipulator Approach. *The International Journal of Robotics Research*, 9(4), 3–21.

Xu, Y. and Kanade, T. (eds.) (1993). *Space Robotics: Dynamics and Control*. The Kluwer International Series in Engineering and Computer Science. Springer US, Boston, MA.